

Potential surfaces and delocalization of excitons in dimers

W. J. D. Beenken, M. Dahlbom, P. Kjellberg, and T. Pullerits

Department of Chemical Physics, Lund University, Lund, Sweden

(Received 22 March 2002; accepted 2 July 2002)

In the present work we will demonstrate that the nuclear dynamics have a strong influence on the delocalization of an exciton in a dimer, even if they do not effect the excitonic interaction. It will be shown that the internal nuclear conformation of the molecules forming the dimer depends critically on the delocalization of the exciton state in the dimer and vice versa. The resulting closed loop enforces a localization of the lower excitonic state, but, contrary to the commonly accepted view, a delocalization of the upper one. Qualitatively different time-evolution of the delocalization length for the lower and upper excitonic state will be shown. Besides, it will turn out that the nuclear motions inhibit a complete delocalization of the excitonic state in any case. To accomplish nuclear and exciton dynamics, the nonadiabatic coupling between the two excitonic states will be deduced. This causes a relaxation from the upper to the lower excitonic state, which limits the maximum reachable exciton delocalization. © 2002 American Institute of Physics.

[DOI: 10.1063/1.1502647]

I. INTRODUCTION

Electronic excited states of interacting molecular systems has been an active research area since early work by Frenkel.¹ The concept of collective delocalized excitations, excitons, was developed. Phenomena like Davydov splitting in molecular crystals,² motional narrowing in molecular aggregates,^{3–5} superradiant decay in molecular aggregates,⁶ and photosynthetic light-harvesting antenna systems,⁷ to name a few, have been explained by using the exciton theory. Particularly the excitons in antenna systems has been recently in the focus of active research.⁸ Such issues as exciton relaxation,^{9–12} excitation delocalization versus localization,^{13–16} and the resulting spectroscopic signatures¹⁷ has been addressed.

Already Frenkel recognized the important role of the nuclear motions in the concept of excitons.¹ First of all, even a weak coupling of the electronic and nuclear degrees of freedom causes dephasing and population relaxation among exciton levels (cf. Ref. 18). For strong electron–phonon coupling, further phenomena like self-trapping of the exciton, also called polaron formation, occur.^{19–21} Various theoretical approaches addressing different aspects of exciton dynamics in antenna systems have recently appeared. For example, Redfield relaxation theory, has been applied using model functions^{22–24} as well as experimental data²⁵ for the spectral density to describe exciton relaxation and corresponding experimental observables in different antenna systems. Förster transfer theory^{26,27} has been extended to account for the transfer to delocalized states with very weak collective transition dipole moments, which still can have a significant Coulombic interaction with the donor if one goes beyond point–dipole approach.^{28,29} Theoretical studies have also addressed the issue of polaron formation in photosynthetic light harvesting.^{30,31} Particularly, for the peripheral light harvesting antenna (LH2) of purple bacteria all above processes have been identified; for a review, see Ref. 32. Exciton re-

laxation in LH2 has been reported by a number of authors.^{10,11,33} The low temperature long wavelength spectral features of transient absorption measurements of LH2 have been assigned to the red stimulated emission indicating polaron formation in these systems.^{34,35} Very recently the same interpretation was given to explain the low temperature selectively excited fluorescence spectra of LH2.³⁶

In order to describe simultaneously different stages of exciton dynamics we have recently developed a method³⁷ based on nuclear dynamics for explicit vibrational modes combined with the surface hopping approach.³⁸ In this method the complete dynamic process from dephasing and exciton relaxation to polaron formation (self-trapping), and eventually diffusion of the polaron can be described. This approach seems to be appropriate for application on excitonically coupled systems of arbitrary size, from the simple dimer to the extended photosynthetic antenna complexes mentioned above. Even the excitonic dynamics of the simplest possible system, the molecular dimer, are of interest. There exist a large variety of dimeric molecular systems from interacting pair of guest molecules in a molecular mixed crystal³⁹ to dimeric pigment complexes in biological systems like a so called B820 antenna complex from purple bacteria⁴⁰ and a special pair of the photosynthetic reaction center.⁴¹ Excited states and their dynamics in molecular dimers has been studied experimentally and theoretically by numerous authors.^{42–48} The list of references can be significantly longer here.

Based on the previous work of Witkowski and Moffitt,⁴⁹ Fulton and Gouterman demonstrated the mathematical treatment of the vibronic and excitonic coupling in a homodimer with one vibrational mode per monomer.⁵⁰ They applied the symmetry of the problem to solve the quantum mechanical eigenvalue problem for the vibrations and determine stick spectra⁴³ for the corresponding vibrational progressions. For the same problem (homodimer) Hayashi *et al.*⁴⁴ determined the adiabatic potential surfaces, explicitly. In the present

work we will extend these calculations of potential surfaces to the more general case of the heterodimer, where the transition energies of the two molecular sites are different. Furthermore, different from the previous works, we will use a quantum-classical approach to describe the nuclear motion in a dissipative surrounding by a Langevin equation.^{51,52} Our aim is to correlate the nuclear motion on the potential surfaces to the exciton delocalization, which is of relevance for absorption, fluorescence, and energy transfer in molecular aggregates. Thereby it will arise that contrary to the commonly accepted view the nuclear dynamics can result in an increase of the delocalization for the upper exciton state. The time evolution of the delocalization will be demonstrated for the two exciton states separately as well as for the case including the nonadiabatic coupling between them, which results in exciton relaxation.

Finally we will give two examples from photosynthetic antennas containing dimeric chlorophyll subunits.

II. POTENTIAL SURFACES

According to the Born–Oppenheimer approximation the electronic motion has been separated from the nuclear motion. For the single molecule the electronic states $|\mu\rangle$ result from solving the stationary Schrödinger equation, which also yields the electronic eigenenergies $E_\mu(\cdots\mathbf{R}_k\cdots)$. Both, the states and the eigen-energies depend parametrically on the nuclear coordinates \mathbf{R}_k . This dependence defines the adiabatic potential surface $U_\mu(\cdots\mathbf{R}_k\cdots)$ of electronic state $|\mu\rangle$. For sake of simplicity we will model the molecular electronic system as a two-level system with a ground state $|g\rangle$ and an excited state $|e\rangle$. For the ground state potential surface the minimum energy nuclear configuration is $\mathbf{R}_k^{(0)}$ and the displacements $\mathbf{R}_k - \mathbf{R}_k^{(0)}$ have been transformed to dimensionless normal coordinates q_ξ . Neglecting anharmonicity terms one obtains the adiabatic potential surface of the electronic ground state as

$$U_g(\cdots q_\xi \cdots) = U_0 + \frac{1}{2} \sum_\xi \hbar \omega_\xi q_\xi^2, \quad (1)$$

where ω_ξ is the oscillator mode frequency and $U_0 = U_g(\cdots \mathbf{R}_k^{(0)} \cdots)$ the minimum energy. For further simplification we will assume that the excited state potential surface is given by the shifted ground state potential surface as

$$U_e(\cdots q_\xi \cdots) = U_0 + \hbar \omega_{eg} + \frac{1}{2} \sum_\xi \hbar \omega_\xi (q_\xi^2 - 2d_\xi q_\xi), \quad (2)$$

where d_ξ represents the origin-shift and ω_{eg} the electronic transition frequency for the nuclear configuration $\mathbf{R}_k = \mathbf{R}_k^{(0)}$, i.e., all $q_\xi = 0$. We will limit the number of explicit intramolecular modes to one per monomer site ($\xi = j$) in what follows. Thus the ground state potential surface $U_g(q_1, q_2)$ for a dimer is simply a paraboloid centered at $(q_1, q_2) = (0, 0)$.

For the excited states of the dimer we have to take into account the excitonic interaction between the transition dipoles $\boldsymbol{\mu}_i$, usually described in the point–dipole approximation as

$$\hbar J_{ij} = \frac{\boldsymbol{\mu}_i \boldsymbol{\mu}_j}{R_{ij}^3} - 3 \frac{(\boldsymbol{\mu}_i \mathbf{R}_{ij})(\boldsymbol{\mu}_j \mathbf{R}_{ij})}{R_{ij}^5} \quad \text{for } i \neq j. \quad (3)$$

If the intermolecular distance R_{ij} is very small, one has to go to a description of the Coulomb interaction beyond the dipole–dipole ansatz⁵³ and probably also to include the exchange interaction term. This can be easily done in our approach by a proper choice of the excitonic interaction matrix element J_{ij} . In what follows, we assume that the excitonic coupling $\hbar J_{ij}$ does not depend on the vibrational modes. Combining the off-diagonal matrix elements $\hbar J_{ij}$ with the diagonal matrix elements H_{jj} represented by the potential surfaces $U_{e,j}(\cdots q_i \cdots)$ of the excited site j and $U_{g,k}(\cdots q_k \cdots)$ for those sites in the ground state, the one-exciton Hamiltonian in site representation is

$$H_{ij} = \hbar \left(\omega_{eg,i} + \frac{1}{2} \sum_k \omega_k q_k^2 - \omega_j d_j q_j \right) \delta_{ij} + \hbar J_{ij} (1 - \delta_{ij}). \quad (4)$$

Here, we have set $U_0 = 0$. The diagonalization of the Hamiltonian H_{ij} results in the eigen-energies of collective excited states—the excitons. For the case of a dimer, with different site energies ω_{eg1} and ω_{eg2} but the same vibrational mode frequencies ω and origin shifts d , the two eigen-energies of the excitons yield as

$$U_\pm(\tilde{q}_1, \tilde{q}_2) = \hbar \omega_{eg} + \frac{\hbar \omega}{2} d^2 (\tilde{q}_1^2 + \tilde{q}_2^2 - \tilde{q}_1 - \tilde{q}_2 \pm \sqrt{(\tilde{q}_2 - \tilde{q}_1 + \Delta)^2 + v^2}) \quad (5)$$

using the normalized dimensionless coordinates $\tilde{q}_j = q_j/d$, the dimensionless excitonic interaction parameter

$$v = \frac{2J_{12}}{\omega d^2} \quad (6)$$

and the dimensionless parameter Δ for the site energy mismatch given as

$$\Delta = \frac{\omega_{eg2} - \omega_{eg1}}{\omega d^2}. \quad (7)$$

The exciton-energies $U_\pm(\tilde{q}_1, \tilde{q}_2)$ represent two-dimensional potential surfaces for the nuclear motion in the dimer with respect to the two explicit intramolecular modes. The physical meaning of the two parameters v and Δ becomes clear once one recognizes the denominators ωd^2 as the Stokes shift, which represents the coupling energy between the electronic and vibrational degrees of freedom.

First we search for the stationary points (minima, maxima and saddle-points) of the potential surface. Since $U_\pm(\tilde{q}_1, \tilde{q}_2)$ depends on the sum $\tilde{q}_1 + \tilde{q}_2$ like a harmonic potential centered at

$$\tilde{q}_1 + \tilde{q}_2 = 1, \quad (8)$$

the stationary points can only occur on the antidiagonal given by Eq. (8). The dependence of $U_\pm(\tilde{q}_1, \tilde{q}_2)$ on the difference of the explicit coordinates $\tilde{q}_2 - \tilde{q}_1$ is not trivial. The number of stationary points depends critically on the interaction parameter v as well as the site energy parameter Δ . In Fig. 1 we have plotted the v -dependence of the stationary

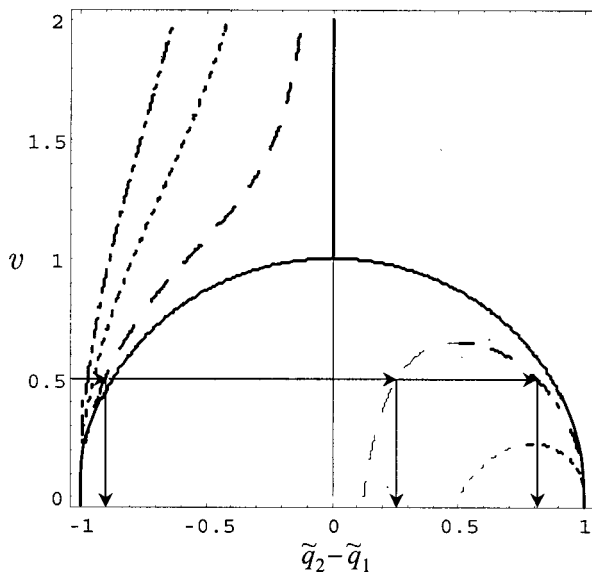


FIG. 1. Positions of the stationary points on the lower potential surface $U_-(\tilde{q}_1, \tilde{q}_2)$ on the antidiagonal $\tilde{q}_1 + \tilde{q}_2 = 1$ given in dependency on the coordinate differences $\tilde{q}_2 - \tilde{q}_1$ and the critical interaction parameter v for several site energy parameter values: $\Delta = 0$ (solid line), $\Delta = 0.1$ (dashed line), $\Delta = 0.5$ (dotted line), and $\Delta = 1$ (dotted-dashed line). The thick lines represent minima, the thin lines represent saddle-points. The arrows illustrate the method described in the text to find the stationary points for $v = 0.5$ and $\Delta = 0.1$.

points of the lower exciton potential surface $U_-(\tilde{q}_1, \tilde{q}_2)$ for several positive site energy parameters Δ . In order to obtain the positions of the stationary points, one has to choose the horizontal line (horizontal arrows in Fig. 1) which represents the given value of the interaction parameter v . Then one has to search for the intersections with the line that represents the given site energy mismatch, e.g., the dashed line for $\Delta = 0.125$. Together with the condition that all extrema have to lie on the line $\tilde{q}_1 + \tilde{q}_2 = 1$, see above, the obtained values $\tilde{q}_1 - \tilde{q}_2$ (vertical arrows) give one the stationary points in the $(\tilde{q}_1, \tilde{q}_2)$ plane. The first intersection point from the left represents a minimum (thick line), the second, provided three intersections exist, a saddle-point (thin line), and the third a second minimum (thick line).

If the parameters fulfill the equation

$$v^{2/3} + \Delta^{2/3} = 1, \quad (9)$$

one obtains only two stationary points. In this case the stationary point belonging to the second intersection in Fig. 1 represents a flat-point since first and second derivative of U_- in $\tilde{q}_2 - \tilde{q}_1$ become zero. The special case $v = 1$ and $\Delta = 0$ which represents the critical homodimer [see Fig. 2(a)] results in a single minimum at $\tilde{q}_1 = \tilde{q}_2 = 0.5$, which is also a flat point. For $\Delta \neq 0$ [e.g., in Fig. 2(h)] the minimum and the flat point do not coincide. In all supercritical cases, i.e., for $v^{2/3} + \Delta^{2/3} > 1$ [e.g., in Figs. 2(b), 2(c), and 2(e)] one obtains only one single minimum, but no flat point. For the subcritical cases, i.e., $v^{2/3} + \Delta^{2/3} < 1$, however, one obtains two minima [see Figs. 2(d), 2(f) and 2(g)]. They are only for $\Delta = 0$ [see Fig. 2(d)] symmetrical with respect to the diagonal $\tilde{q}_1 + \tilde{q}_2 = 1$. For $\Delta > 0$ there exists always only one global minimum, while the other minimum is metastable.

For the potential surface $U_+(\tilde{q}_1, \tilde{q}_2)$, which belongs to the upper exciton, only one single stationary point exists for all choices of the parameters v and Δ (see Figs. 3 and 4). This means that one obtains always a minimum. For $\Delta > 0$ it is shifted to values of $\tilde{q}_2 - \tilde{q}_1 > 0$, i.e., the direction away from the global minimum of the lower exciton potential surface (cf. Fig. 2). This is very important for the delocalization and localization of the excitons, as one will see below. In the limit $v, \Delta \rightarrow 0$, the potential surface for the upper exciton state $|+\rangle$ is formed by the truncated upper parts of two intersecting paraboloids, resulting in biconical isoenergetic contours [see Fig. 4(f)]. The intersection-line given by $\tilde{q}_1 = \tilde{q}_2$ represents a sharp notch, and is coincident to the sharp ridge on the lower exciton potential surface [cf. Fig. 2(f)].

III. DELOCALIZATION

For an excitonically coupled dimer the upper and lower one-exciton states $|+\rangle$ and $|-\rangle$, respectively, are represented by a superposition of the excited states of the sites $|1\rangle$ and $|2\rangle$ as

$$|\pm\rangle = c_{1\pm}|1\rangle + c_{2\pm}|2\rangle, \quad (10)$$

where the coefficients $c_{i\pm}$ are components of the eigenvectors of the excitonic Hamiltonian. They are given as

$$\begin{pmatrix} c_{1\pm} \\ c_{2\pm} \end{pmatrix} = \frac{1}{\sqrt{N_{\pm}}} \begin{pmatrix} (\tilde{q}_2 - \tilde{q}_1 + \Delta) \pm \sqrt{v^2 + (\tilde{q}_2 - \tilde{q}_1 + \Delta)^2} \\ v \end{pmatrix} \quad (11)$$

normalized by

$$N_{\pm} = v^2 + ((\tilde{q}_2 - \tilde{q}_1 + \Delta) \pm \sqrt{v^2 + (\tilde{q}_2 - \tilde{q}_1 + \Delta)^2})^2. \quad (12)$$

All coefficients $c_{1\pm}$ and $c_{2\pm}$ depend only on the difference of the dimensionless normal coordinates $\tilde{q}_1 - \tilde{q}_2$ but not on the sum $\tilde{q}_1 + \tilde{q}_2$. This means that the character of the exciton can be only changed by nuclear motions perpendicular to the diagonal of the (q_1, q_2) plane, given by $q_1 = q_2$. We will define the delocalization length of the exciton L_{\pm} by the inverse participation ratio¹⁶ as

$$L_{\pm}^{-1} = \sum_j |c_{j\pm}|^4. \quad (13)$$

For the dimer the delocalization length of the one-exciton states can be expressed as

$$L_{\pm}(\tilde{q}_1, \tilde{q}_2) = 1 + \frac{2v^2(\tilde{q}_2 - \tilde{q}_1 + \Delta \pm \sqrt{v^2 + (\tilde{q}_2 - \tilde{q}_1 + \Delta)^2})^2}{v^4 + (\tilde{q}_2 - \tilde{q}_1 + \Delta \pm \sqrt{v^2 + (\tilde{q}_2 - \tilde{q}_1 + \Delta)^2})^4}. \quad (14)$$

The delocalization length for both one-exciton states are equal and depends only on $|\tilde{q}_1 - \tilde{q}_2|/v$. In Fig. 5 the lines of constant delocalization length L_{\pm} are shown on the $(\tilde{q}_1, \tilde{q}_2)$ plane for the homodimer, i.e., $\Delta = 0$, in the critical case $v = 1$. One can see that full delocalization is reached along the diagonal $\tilde{q}_1 = \tilde{q}_2$, where $L_{\pm}(\tilde{q}_1, \tilde{q}_2) = 2$. At increasing $\tilde{q}_2 - \tilde{q}_1$, the delocalization length decreases towards an asymptotic value of $L_{\pm}(\tilde{q}_1, \tilde{q}_2) = 1$ for $|\tilde{q}_1 - \tilde{q}_2| \rightarrow \infty$. The critical parameter v is only scaling the dependency of the delocalization length on the distance $|\tilde{q}_1 - \tilde{q}_2|$. For $v > 1$ the

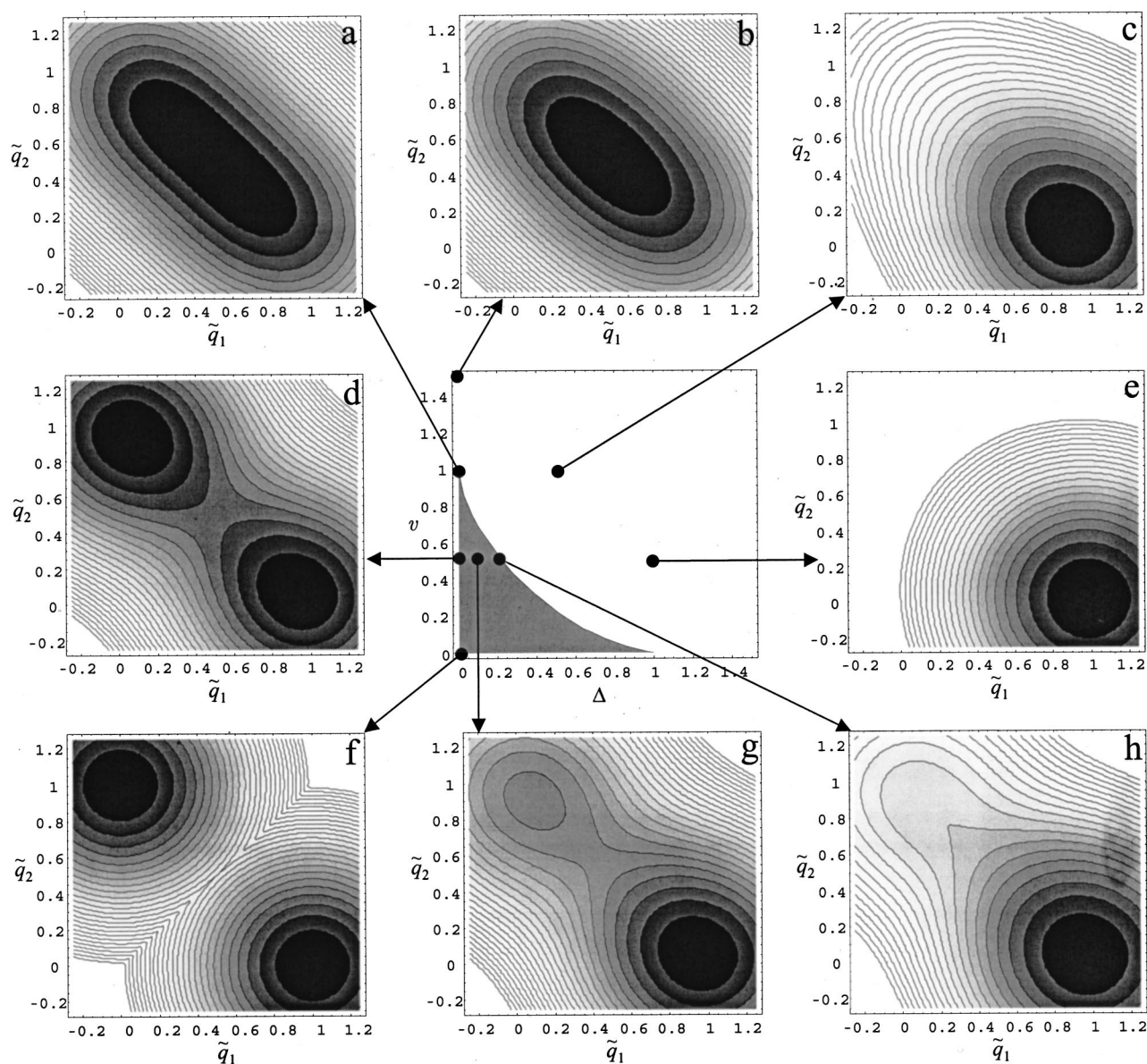


FIG. 2. The lower exciton potential surfaces $U_-(\tilde{q}_1, \tilde{q}_2)$ (panels a–h) for several combinations of the parameters v and Δ displayed in the central diagram, where the shaded area assigns the subcritical cases with $v^{2/3} + \Delta^{2/3} < 1$. Isocontours for each $0.05\hbar\omega d^2$ up to $\hbar\omega d^2$ above the minimum are not shown. Darker shading means lower value.

delocalization ridge is broader, while for $v < 1$ it is narrower than in the critical case. For $v \rightarrow 0$, this means the vibrational coupling is much stronger than the excitonic, one obtains $L_{\pm}(\tilde{q}_1, \tilde{q}_2) = 1$ for all points in the $(\tilde{q}_1, \tilde{q}_2)$ plane except of the line $\tilde{q}_1 = \tilde{q}_2$, where $L_{\pm}(\tilde{q}_1, \tilde{q}_2)$ jumps abruptly to a value of 2. In the limit $v \rightarrow \infty$ one obtains $L_{\pm}(\tilde{q}_1, \tilde{q}_2) \rightarrow 2$ for all points in the $(\tilde{q}_1, \tilde{q}_2)$ plane, meaning an ubiquitous delocalization of the exciton. For the case of the heterodimer, i.e. $\Delta \neq 0$, the maximum value $L_{\pm} = 2$ is reached for the diagonal $\tilde{q}_1 + \tilde{q}_2 = -\Delta$. For $\Delta > 0$ this means a shift of all contours in Fig. 5 to the left upper corner, for $\Delta < 0$ to the right bottom corner. Despite this shift, the slope of $L_{\pm}(\tilde{q}_1, \tilde{q}_2)$ is the same as in Fig. 5.

If one compares the value of the delocalization length $L_{\pm}(\tilde{q}_1, \tilde{q}_2)$ at the global minimum of the one-exciton potential surfaces with that at the ground state minimum $L_{\pm}(0, 0)$ one can state:

(i) For the lower exciton state the delocalization length will always decrease when approaching the global minimum (see Fig. 6). For $\Delta \ll v < 1$, which means the subcritical case of nearly a homodimer, one obtains a significant loss of delocalization. In this case, the initial nuclear conformation corresponds to an almost fully delocalized exciton state. However, the global minimum of the potential surface, which the nuclear configuration moves to, corresponds to a nearly localized exciton, as mentioned above. Especially, in the extreme case $\Delta = 0$ (homodimer) and $v \rightarrow 0$ (vanishing excitonic coupling) the initial total delocalization of the exciton will be destroyed completely, i.e., $\Delta L_- = -1$. For other values of the parameters v and Δ the loss of delocalization length is smaller. On the one hand, in the supercritical case $v > 1 > \Delta$ (homodimerlike), for both, the initial and final nuclear configuration, the distance to the diagonal given by $\tilde{q}_1 = \tilde{q}_2$ is too similar to cause significantly different delocal-

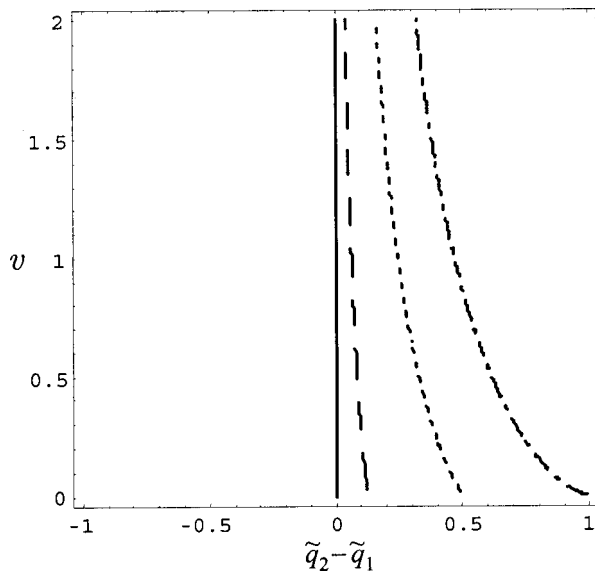


FIG. 3. Positions of the stationary point (minimum) on the upper potential surface $U_+(\tilde{q}_1, \tilde{q}_2)$ on the anti-diagonal $\tilde{q}_1 + \tilde{q}_2 = 1$ given in dependency on the coordinate differences $\tilde{q}_2 - \tilde{q}_1$ and the critical interaction parameter v . For further explanation see text and Fig. 1.

ization lengths. On the other hand, in the supercritical case $\Delta > 1 > v$ (extreme heterodimer), there exists no initial delocalization to be lost.

(ii) For the upper exciton state the delocalization length will always increase, as shown in Fig. 7. The reason for this behavior is that the single minimum of the upper potential surface lies always between the diagonal given by $\tilde{q}_2 = \tilde{q}_1$ and the line of maximum delocalization length given by $\tilde{q}_1 = \tilde{q}_2 + \Delta$. The reason for the smaller gain of delocalization in the case $v \gg \Delta$ is that the initial state has nearly the maximum delocalization length $L_+ = 2$. For $\Delta > v$ and $\Delta > 1$ the smaller gains in delocalization results from the fact that the excitonic interaction is not able to compensate the site energy mismatch.

IV. NUCLEAR DYNAMICS

In the previous section, we have studied the delocalization of an one-exciton state in the relaxed nuclear configuration. Here we will demonstrate, how the system moves from the initial to the final nuclear conformation. Furthermore, we will show the fluctuating nuclear dynamics around the minimum of the potential surfaces, particularly the zero-point motion. These fluctuations are of great importance influencing the effective delocalization length. In the subcritical case for the lower exciton they can cause transitions of the nuclear configuration from one minimum of the potential surface to the other. To take thermal as well as zero-point motion into account, we will use a quantum-classical description of the nuclear motion on the potential surface. This approach is easier to handle than the nuclear wave-packet propagation and sufficient for dissipative quantum systems based on harmonic oscillator potentials.^{51,52,54}

In dimensionless normal coordinates \tilde{q}_j the Hamiltonian for the nuclear motion is given as

$$H_{\pm\pm} = \frac{\hbar \omega d^2}{2} \sum_j \tilde{p}_j^2 + U_{\pm}(\cdots \tilde{q}_j \cdots), \quad (15)$$

where the \tilde{p}_j represent the normalized dimensionless nuclear momenta, quantum-mechanically given as

$$\tilde{p}_j = \frac{1}{d^2} \frac{\partial}{\partial \tilde{q}_j}. \quad (16)$$

It has to be noted that the Hamiltonian for the nuclear motion in general will not be diagonal in the exciton representation, since the operator $\sum_j \tilde{p}_j^2$ may not be diagonal in this representation (see below). For the time being, we will neglect the off-diagonal matrix elements H_{+-} . This means use the adiabatic approximation. The effects resulting from the off-diagonal matrix elements H_{+-} , consequently called nonadiabatic couplings, will be discussed subsequently.

For the quantum-classical description of the nuclear motion on the potential surface $U_{\pm}(\cdots \tilde{q}_j \cdots)$, one can use the quantum-statistical expectation values of the coordinates \tilde{q}_i and the momenta \tilde{p}_i . Their time evolutions are ruled by the canonical equations given as

$$\frac{\partial \tilde{q}_i}{\partial t} = \frac{1}{\hbar d^2} \frac{\partial H_{\pm\pm}}{\partial \tilde{p}_i} = \omega \tilde{p}_i, \quad (17)$$

$$\frac{\partial \tilde{p}_i}{\partial t} = -\frac{1}{\hbar d^2} \frac{\partial H_{\pm\pm}}{\partial \tilde{q}_i} = F_{\pm,i}(\tilde{q}_1, \tilde{q}_2). \quad (18)$$

The second canonical equation defines the forces $F_{\pm,i}(\tilde{q}_1, \tilde{q}_2)$ as the negative gradient of the potential surface $U_{\pm}(\cdots \tilde{q}_j \cdots)$. For the one-exciton states these are given as

$$F_{\pm,1}(\tilde{q}_1, \tilde{q}_2) = \omega \left(\frac{1}{2} - \tilde{q}_1 \right) \pm \frac{\omega}{\sqrt{(\tilde{q}_2 - \tilde{q}_1 + \Delta)^2 + v^2}} \quad (19)$$

and $F_{\pm,2}(\tilde{q}_1, \tilde{q}_2)$, analogously. It is the second term in Eq. (19), which is specific for the one-exciton states, $|+\rangle$ and $|-\rangle$. It can give rise to both localization and delocalization of the exciton. Depending on its sign it can amplify or compensate the generally delocalizing first term in Eq. (19). Especially, if it overcompensates the first term this will result in the subcritical cases where two minima occur on the potential surface. Due to the sign of the second term in Eq. (19), this can happen only for the lower exciton state $|-\rangle$, as shown in Fig. 2.

To describe the nuclear motion in terms of the explicit coordinates \tilde{q}_i including a dissipative bath of modes as surrounding, one can use the Langevin equation,⁵¹ which is given as

$$\frac{\partial^2 \tilde{q}_i}{\partial t^2} - \omega F_{\pm,i}(\tilde{q}_1, \tilde{q}_2) = -\gamma \frac{\partial \tilde{q}_i}{\partial t} + \omega f_i(t). \quad (20)$$

The left-hand side of Eq. (20) represents the canonical equation for the explicit mode as given in Eqs. (17) and (18), including the forces resulting from excitonic polaron formation, as given in Eq. (19). The right-hand side represents additional forces resulting from the interaction between the explicit modes with the surrounding thermalized bath. The first term on the right-hand side, containing the parameter γ , gives a damping of the explicit mode motion by friction, the

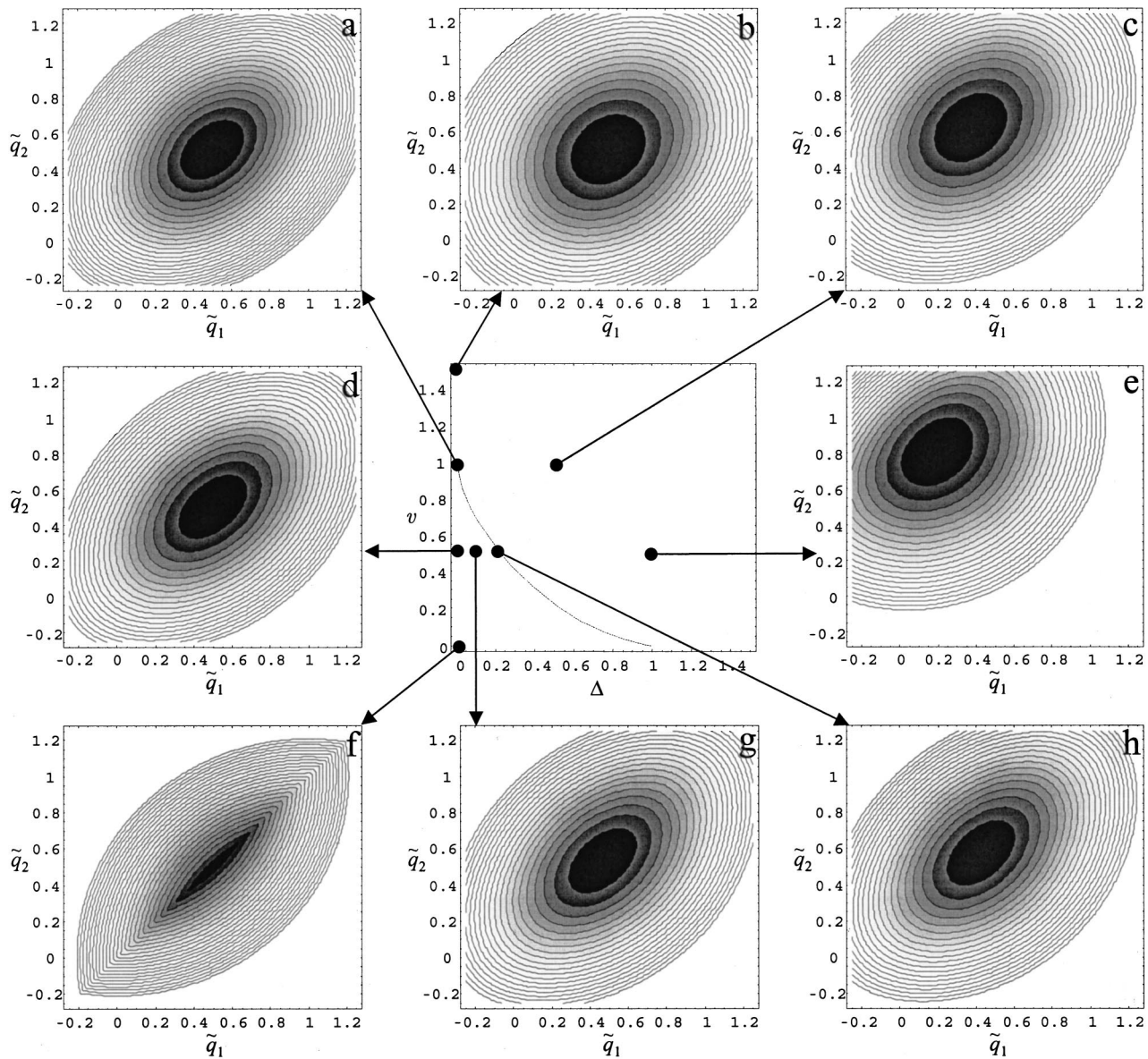


FIG. 4. The upper exciton potential surfaces $U_+(\tilde{q}_1, \tilde{q}_2)$ for several combinations of the parameters v and Δ displayed in the central diagram. For the sake of comparison the critical line $v^{2/3} + \Delta^{2/3} = 1$ is indicated. For further explanations see text and Fig. 2.

second term represents fluctuating forces. Without the fluctuating forces $f_i(t)$, the damping term in Eq. (20) results in nuclear motion towards one of the minima of the potential surface. However, the fluctuating forces $f_i(t)$, cannot be switched off, since they are an expression of the microscopic thermodynamical kinetics. According to the dissipation fluctuation theorem^{51,55} the variances of the fluctuating forces, given as $\langle f_i^2 \rangle$, are connected with the damping by

$$\langle f_i^2 \rangle = \frac{2\gamma}{\tau^*} \langle \tilde{p}_i^2 \rangle = \frac{2\gamma}{\tau^* d^2} \left(n(\omega, T) + \frac{1}{2} \right), \quad (21)$$

where τ^* represents the bath correlation time. The Bose-Einstein distribution $n(\omega, T)$ and the summand $\frac{1}{2}$ take into account the thermal and zero-point energy, respectively. The latter means that even for $T \rightarrow 0$ K the fluctuating forces will result in a nuclear zero-point motion. It has to be noted that

we use normalized dimensionless momenta [see Eq. (16)]. Therefore the fluctuating forces f_i scale with d^{-1} .

Because of the fluctuating forces $f_i(t)$ the nuclear conformation $(\tilde{q}_1, \tilde{q}_2)$ moves like a Brownian particle on the potential surface. Consequently the (de)localization of the exciton is now a statistical quantity. Using the distribution $N_{\pm}(\tilde{q}_1, \tilde{q}_2; t)$, which gives the probability to find a nuclear conformation $(\tilde{q}_1, \tilde{q}_2)$ at time t , the effective delocalization length is given by

$$L_{\pm, \text{eff}}(t) = \int \int L_{\pm}(\tilde{q}_1, \tilde{q}_2) N_{\pm}(\tilde{q}_1, \tilde{q}_2; t) d\tilde{q}_1 d\tilde{q}_2. \quad (22)$$

In order to determine the time evolution of the effective delocalization length $L_{\pm, \text{eff}}(t)$ we have performed Monte Carlo simulations of 400 000 trajectories. In Fig. 8, choosing a displacement of $d=2$ and considering only the zero-point

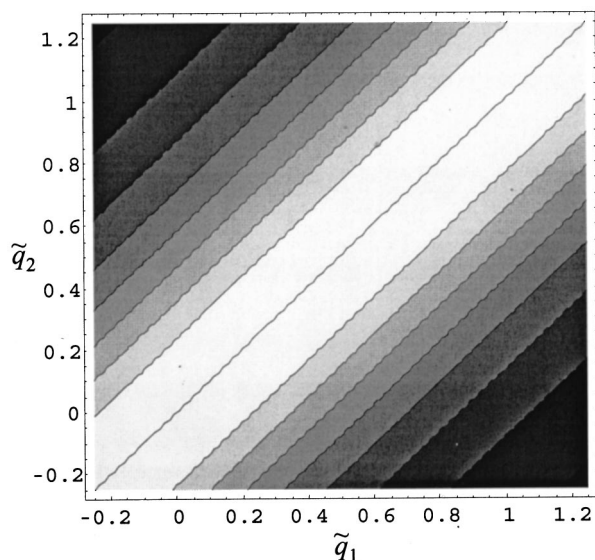


FIG. 5. Delocalizations length $L_{\pm}(\tilde{q}_1, \tilde{q}_2)$ plotted over the $(\tilde{q}_1, \tilde{q}_2)$ -plane for the critical case of the homodimer $v=1$. Contours are displayed in steps of $\Delta L_{\pm}(\tilde{q}_1, \tilde{q}_2)=0.1$. The shading becomes darker for lower values of $L_{\pm}(\tilde{q}_1, \tilde{q}_2)$. The maximum value $L_{\pm}(\tilde{q}_1, \tilde{q}_2)=2$ is reached along the diagonal $\tilde{q}_1=\tilde{q}_2$, the minimum $L_{\pm}(\tilde{q}_1, \tilde{q}_2)=1$ is asymptotic for $|\tilde{q}_2-\tilde{q}_1|\rightarrow\infty$.

motions ($T\rightarrow 0$ K) the final distributions $N_{-}(\tilde{q}_1, \tilde{q}_2; t\rightarrow\infty)$ are displayed for the lower exciton state. As one can see, the contours follow those of the corresponding potential surface (cf. Fig. 2). For sections parallel to the diagonal $\tilde{q}_1=\tilde{q}_2$, the slope of the distribution is a Gaussian as one can expect for the ground state of a harmonic oscillator potential. The noise in the distributions reflects the fluctuations of the motion.

The time evolution of the effective delocalization lengths $L_{\text{eff-}}$ of the lower exciton are shown in Fig. 9 for the parameter sets used in Figs. 2 and 8. The time t is presented in units of the inverse vibrational frequency ω^{-1} . The exciton local-

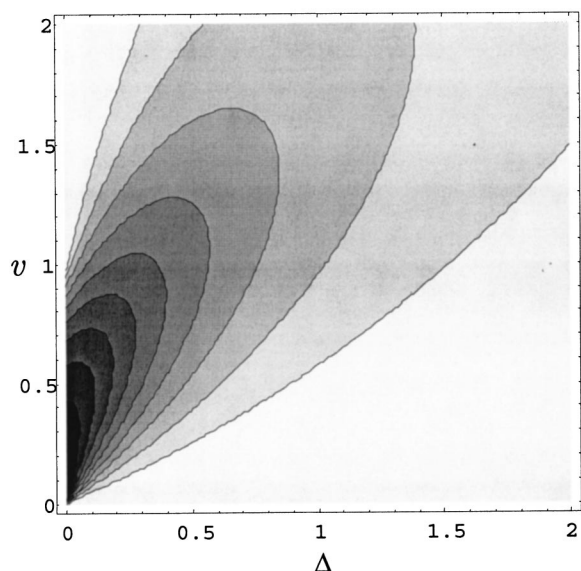


FIG. 6. Decrease of the delocalization length $L_{-}(\tilde{q}_1, \tilde{q}_2)$ for the lower exciton state by polaron formation, from $\Delta L_{-}=0$ (white) until $\Delta L_{-}=-1$ (black), in dependence of the interaction parameter v and the site energy parameter Δ .

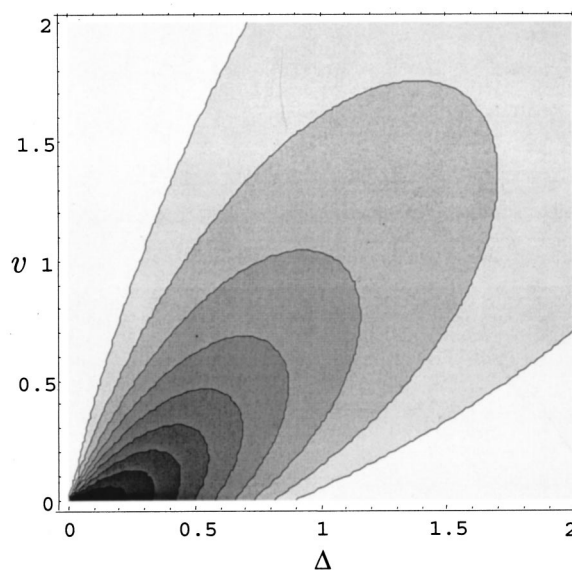


FIG. 7. Increase of the delocalization length $L_{+}(\tilde{q}_1, \tilde{q}_2)$ for the upper exciton state by polaron formation, from $\Delta L_{+}=0$ (white) until $\Delta L_{+}=0.5$ (darkest shading), in dependence of the interaction parameter v and the site energy parameter Δ .

izes with time, as expected (cf. Fig. 6). In the case of the homodimer (a, b, d) the initial delocalization length is lower than two due to the finite width of the initial distribution $N_{-}(\tilde{q}_1, \tilde{q}_2; 0)$. For supercritical homodimers (a, b), where the excitonic coupling is stronger than the electron–vibration coupling ($v\geq 1$), the delocalization length does not change a lot. A localization occurs only because the final distribution $N_{-}(\tilde{q}_1, \tilde{q}_2; \infty)$ is broader than the initial $N_{-}(\tilde{q}_1, \tilde{q}_2; 0)$ for $d>1$.

For the subcritical homodimer (d) as well as for heterodimers with moderate site energy mismatch (c, h) the localization of the exciton with time is much more significant, since here the whole distribution $N_{-}(\tilde{q}_1, \tilde{q}_2; t)$ drifts away from the line of maximum delocalization, towards the potential surface minima. If both, excitonic coupling and site energy mismatch are greater than the electron–vibration coupling (e) the delocalization length starts already at a low value, i.e., the exciton is localized all the time. In the opposite case $v=\Delta\rightarrow 0$ (f; not shown in Fig. 9), the effective delocalization lengths is trivially $L_{\text{eff-}}=1$, since the area for $L_{-}(\tilde{q}_1, \tilde{q}_2)>1$ is infinitesimally small.

The time evolution of the effective delocalization lengths for the upper exciton state ($L_{\text{eff+}}$) are shown in Fig. 10. Contrary to the commonly accepted view that dynamic disorder leads to a localization of the excitation, here the delocalization length increases, particularly for the heterodimers (c, e, h). This means that the nuclear dynamics (dynamic disorder) can compensate the localization effect of the site energy mismatch (static disorder).

Last but not least, in Fig. 11 the temperature dependence of $L_{\text{eff-}}(t)$ for two different homodimers ($\Delta=0$) is shown. The differences between the supercritical (b) and the subcritical (d) case can be explained by the broadening of the peak(s) of the respective distributions $N_{-}(\tilde{q}_1, \tilde{q}_2; t)$ if the temperature increases. In the supercritical case (b) a broader

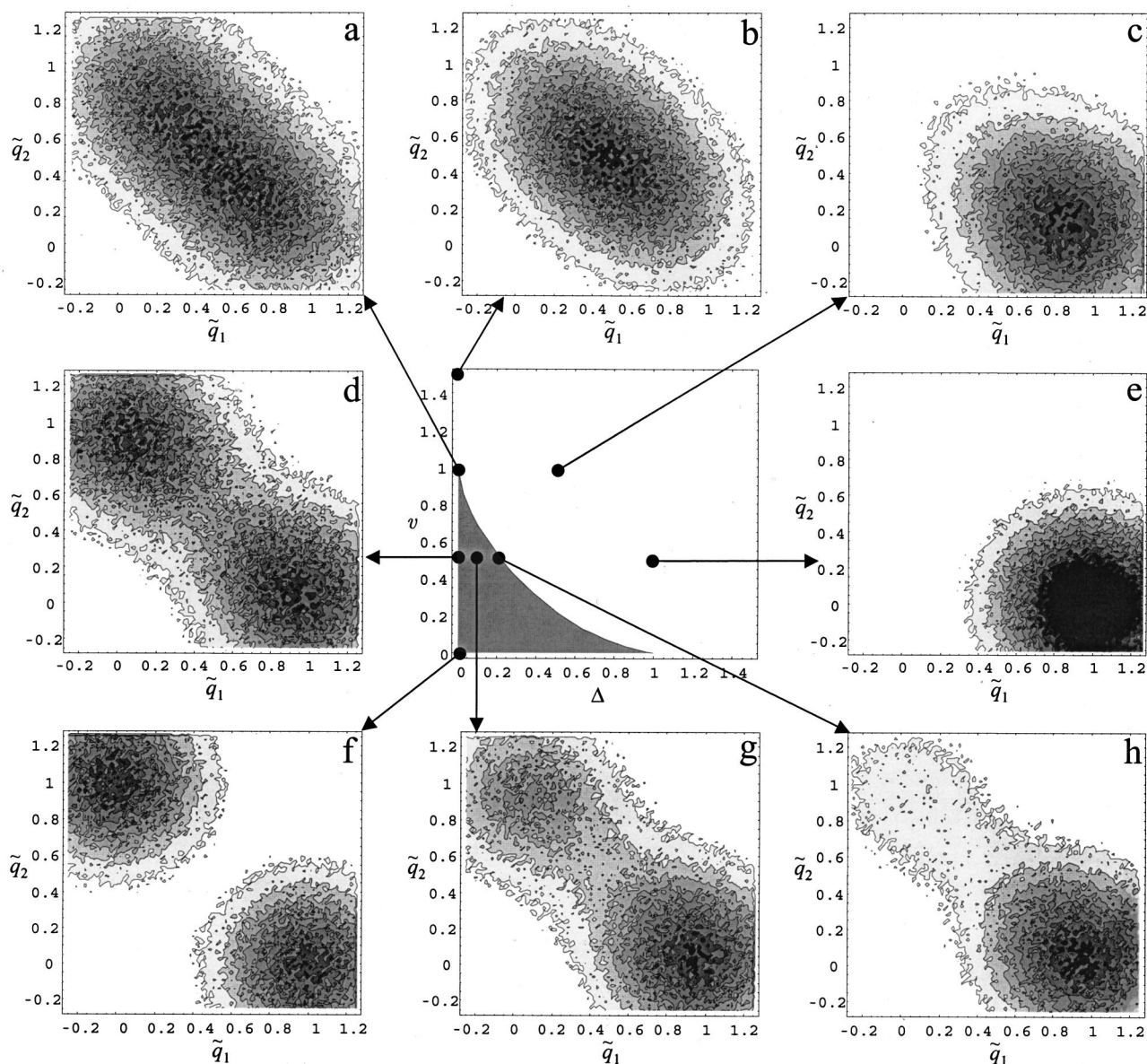


FIG. 8. Final distributions $N_-(\tilde{q}_1, \tilde{q}_2)$ for the lower energetic exciton for several combinations of parameters ν and Δ at temperature $T \rightarrow 0$. The distributions are normalized to their maximum value 1 (black). For further explanation, see text and Fig. 2.

peak centered at $(0.5, 0, 5)$ results in a smaller effective delocalization length, as one can imagine by mapping the distribution $N_-(\tilde{q}_1, \tilde{q}_2; t)$ on the delocalization function $L_-(\tilde{q}_1, \tilde{q}_2)$ (cf. panel b in Fig. 8 with Fig. 5). In the subcritical case, the final distribution $N_-(\tilde{q}_1, \tilde{q}_2; \infty)$ contains two peaks, approximately centered at $(1, 0)$ and $(0, 1)$. If these become broader, they will fill the area between them where the delocalization length is close to the maximum value two (cf. panel d in Fig. 8 with Fig. 5). Therefore the temperature dependence of the final effective delocalization length is weaker in the subcritical case than in the supercritical case. Especially, in a certain range of temperatures the final delocalization may even increase with temperature. One can see that for $T = 0.5\hbar\omega/k$ (dashed curve d in Fig. 11) the final effective delocalization length is slightly larger than for $T = 0$ K (solid line). For higher temperatures ($T > 1\hbar\omega/k$; dashed-dotted curves d), however, the final effective delo-

calization length will always decrease with temperature, though in a lower degree in the subcritical than in the supercritical case.

V. NONADIABATIC COUPLING

In the previous section we have described the nuclear motion on the two-dimensional adiabatic potential surfaces, and the effect of these dynamics on the delocalization. One has to consider, however, that the one-exciton state may not remain on the initial potential surface. A switching between the upper and lower potential surface may occur and is of great interest for the polaron formation process. This switching is caused by nonadiabatic terms of the excitonic Hamiltonian.

Due to Eqs. (10) and (11) it is obvious that not only the electronic energies represented by the potential surfaces

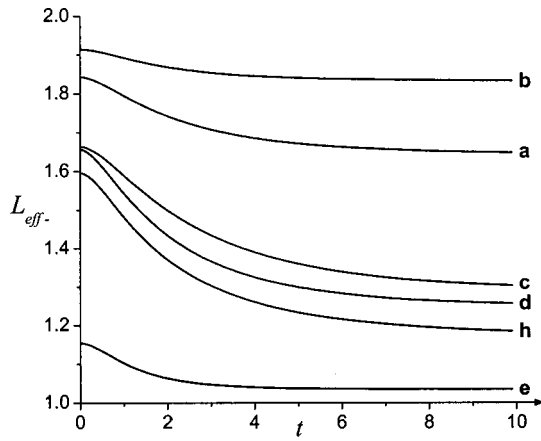


FIG. 9. Time evolution of the effective delocalization length $L_{\text{eff-}}$ in the overdamped case $\gamma=2\omega$ for displacement $d=\sqrt{8}$ and temperature $T \rightarrow 0$ K. The parameter sets (v, Δ) are the same (a–h) as used in Figs. 2 and 8, respectively. The time t is given in units of ω^{-1} .

$U_{\pm}(\tilde{q}_1, \tilde{q}_2)$ but also the exciton states $|\pm\rangle$ themselves depend on the normal coordinates \tilde{q}_1 and \tilde{q}_2 . Therefore one has to consider that the representation of the Hamiltonian H in the adiabatic basis $\{|+\rangle, |-\rangle\}$ does not only consist of the diagonal matrix elements $H_{\pm\pm} = U_{\pm}(\tilde{q}_1, \tilde{q}_2)$, but contains also off-diagonal matrix elements given as

$$H_{+-} = i\hbar\omega \sum_{i,j} c_{i+} \frac{\partial c_{i-}}{\partial \tilde{q}_j} \tilde{p}_j, \quad (23)$$

and represent the nonadiabatic coupling between the exciton states $|+\rangle$ and $|-\rangle$. Since they depend on the nuclear momenta \tilde{p}_j , they cannot be included in a conservative potential, but are connected with such phenomena as energy relaxation and internal conversion. The mixing of the adiabatic exciton states by nonadiabatic couplings H_{+-} can be considered as stochastic instantaneous jumps of the system from one potential surface to the other. The rate of this surface hopping $k_{\pm \rightarrow \mp}$ is related to the non-adiabatic coupling $|H_{+-}|^2$ via Fermi's Golden Rule,

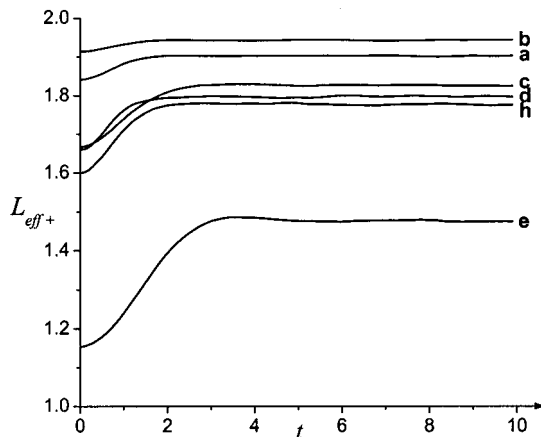


FIG. 10. Time evolution of the effective delocalization length $L_{\text{eff+}}$ for the upper excitonic state $|+\rangle$. Parameters and time scale as in Fig. 9.

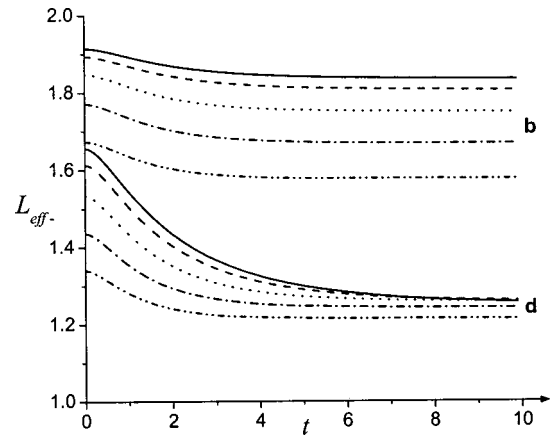


FIG. 11. Time evolution of the effective delocalization length $L_{\text{eff-}}$ of the lower excitonic state $|-\rangle$ for temperatures $T=0$ (solid), $0.5\hbar\omega/k$ (dashed), $\hbar\omega/k$ (dotted), $2\hbar\omega/k$ (dashed-dotted), and $4\hbar\omega/k$ (dashed-dotted-dotted). For parameter sets (b,d) and time scale, see Fig. 9.

$$k_{\pm \rightarrow \mp} = \frac{2\pi}{\hbar} \int |H_{+-}|^2 \delta\left(U_{\pm} - U_{\mp} + \frac{1}{2}\hbar\omega\right) \times \sum_{j=1,2} (p_j'^2 - d^2 p_j^2) dp_1' dp_2', \quad (24)$$

where p_j' and p_j represents the (nonscaled, dimensionless) final and the initial nuclear momenta, respectively. The delta function in Eq. (24) means that after the hopping the excess potential energy $U_{\pm} - U_{\mp}$ has to be taken by kinetic energy of the nuclear motion. The change of the nuclear momenta, $\mathbf{p}' - \mathbf{p}$ is parallel to the nonadiabatic coupling vector,^{38,56} i.e.,

$$p_j' - p_j \propto \sum_i c_{i+} \frac{\partial c_{i-}}{\partial \tilde{q}_j}. \quad (25)$$

For a dimer this means that the momentum change happens in the direction $(1, -1)$. Thus after hopping from the upper to the lower exciton state the (scaled, dimensionless) momenta will rise from $\tilde{p}_{1,2}$ to $\tilde{p}'_{1,2}$ as

$$\tilde{p}'_{1,2} = \frac{\tilde{p}_1 + \tilde{p}_2}{2} \pm \frac{\tilde{p}_1 - \tilde{p}_2}{2} \sqrt{1 + \frac{4\sqrt{v^2 + (\tilde{q}_2 - \tilde{q}_1 + \Delta)^2}}{(\tilde{p}_1 - \tilde{p}_2)^2}}. \quad (26)$$

At low temperatures one needs only the surface hopping rate for the jump from the upper to the lower exciton state given by

$$k_{+\rightarrow-} = \frac{\pi\omega}{2} \left(\frac{v|\tilde{p}_2 - \tilde{p}_1|}{v^2 + (\tilde{q}_2 - \tilde{q}_1 + \Delta)^2} \right)^2. \quad (27)$$

This hopping rate depends on the critical interaction parameter v , momentum $\tilde{p}_2 - \tilde{p}_1$, and the relevant nuclear coordinate $\tilde{q}_1 - \tilde{q}_2 + \Delta$, the latter both parallel to the anti-diagonal given by 8. One can see that the rate $k_{+\rightarrow-}$ increases for approaching to a nuclear configuration where $\tilde{q}_1 - \tilde{q}_2 = \Delta$. For $v \rightarrow 0$ one obtains a singularity there. However, in the case $v=0$ one should describe the motion by two diabatic harmonic potential surfaces, one for each of the non-interacting sites.

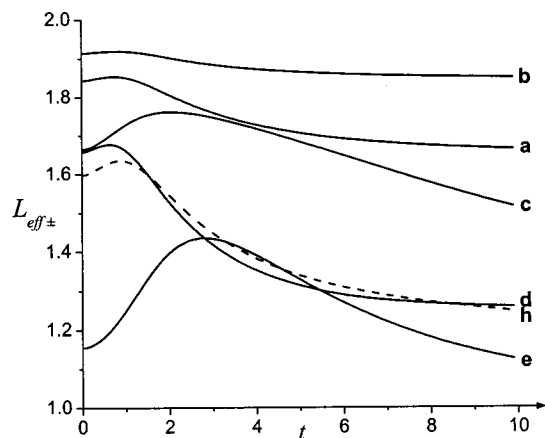


FIG. 12. Time evolution of the effective delocalization length $L_{\pm}(t)$ for a surface hopping system initially prepared in the upper excitonic state $|+\rangle$. Parameters and time scale as in Fig. 9.

In Fig. 12 the time evolution of the effective delocalization length $L_{\pm}(t)$ of a dimer initially prepared in the upper exciton state performing a surface hopping is shown for the sets (a–h) of the parameters v and Δ as used in Fig. 4. One can see that initially the delocalization length rises due to the generally delocalizing forces in the upper exciton state as mentioned above. After a while the system has jumped to the lower exciton state, and localization takes effect. For the heterodimers (c, e, h) the final effective delocalization length (cf. Fig. 9) has been reached significantly later than for the comparable homodimers (a, b, d). The reason is that the nuclear system first searches for the minimum on the upper potential surface, which is situated in a position apart from the diagonal $\bar{q}_2 - \bar{q}_1 + \Delta = 0$. Therefore the hopping rate $k_{+\rightarrow-}$ is smaller than for $\Delta = 0$, where minimum of the upper exciton potential surface and maximum of the hopping rate coincide. Furthermore, after the hopping to the lower exciton state in the heterodimer case ($\Delta \neq 0$) the nuclear system needs to follow a longer track to reach the final minimum potential surface which is diametrically situated to the minimum of the upper exciton potential surface. For the critical case (h) with $v = 0.5$ and $\Delta \approx 0.225$ the latter effect may be more important than the delayed hopping.

VI. CONCLUDING DISCUSSION

In the present work the dynamics of the delocalization of excitons for the homo- as well as heterodimers with one vibrational degree of freedom per monomer have been studied. The minima of the adiabatic potential surface, which have been determined in the usual way,⁴⁴ has been mapped to the delocalization length described as the inverse participation ratio. Instead of solving the nuclear eigenvalue problem,^{43,44} we have simulated the nuclear motion on the potential surfaces by using a quantum-classical approach. The resulting distribution of classical trajectories is comparable to the nuclear wave packet dynamics on a single potential surface in a dissipative surrounding.^{51,52} This distribution enables one to calculate an effective delocalization length $L_{\text{eff}}(t)$. This quantity is a good theoretical measure of the delocalization, since it shows independently of the sym-

metry of the exciton state how many sites participate in the excitonic states in average. Generally it cannot be directly measured. Various other quantities have been suggested to characterize the extent of exciton delocalization. The comparison of them is not always straightforward.¹⁶ For example, the superradiant enhancement L_{sr} depends beside on the extent of delocalization also on the orientations and values of the transition dipoles of the dimer and the population of the excitonic states. Only in special cases, for example a dimer with equal transition dipoles in head-to-tail conformation and only the lower exciton state populated, the superradiant enhancement $L_{\text{sr}}(t)$ directly measures the delocalization dynamics, e.g., in time resolved fluorescence experiments.

Our simulations predict that after excitation from the ground-state (here assumed to be a δ -pulse) the lower exciton state is localizing in any case, while the upper one can be delocalizing in the subsequent time evolution by the nuclear dynamics. Including the nonadiabatic coupling between the potential surfaces, by using the surface hopping method,³⁸ we have shown that after exciting the upper exciton the delocalization length is first increasing according to the exciton-delocalizing tendency of the nuclear dynamics on the upper potential surface, and later decreasing due to the relaxation to the lower exciton potential surface, where the nuclear dynamics gives rise to exciton localization. Thereby, a 30 cm^{-1} mode would result in exciton (de)localization dynamics on a picosecond time scale.

Finally we would like to relate our theoretical results to a few examples from real life. The B820 subunit of the purple bacterial core antenna LH1 is a dimer of bacteriochlorophyll (BChl).⁵⁷ The excitonic coupling in B820 has been estimated to be around 230 cm^{-1} . In order to evaluate the electron-vibration coupling we take a closer look at low temperature fluorescence site selection studies of B820.^{58,59} In these studies the Huang–Rhys factor $S = \frac{1}{2}d^2$ was estimated to be 0.5, i.e., $d \approx 1$. For the phonon frequency ω we take the average of the phonon function, which is about $150\text{--}200 \text{ cm}^{-1}$ and results in an interaction parameter $v \approx 2.5$. If one relates the site energy parameter Δ to the variance of the transition-energy differences between the two BChls of the dimeric subunit, one obtains $\Delta \approx 0.5$. This combination of parameters v and Δ is located above the cases b and c (cf. Fig. 2) and corresponds clearly to a supercritical case with only one minimum on the lower potential surface. Consequently the excitons in the B820 subunit can be described as almost delocalized.

As another example, we take the light harvesting complex two (LHCII) of green plants. There exists no clear dimeric system in LHCII. Nevertheless, the structure suggests that several pairs of chlorophyll molecules (Chl-a and Chl-b) are close together.⁶⁰ For the sites, assigned as Chl-a2 and Chl-b2, one could estimate a distance of about 10 \AA . For a nearly in-line geometry of the transition dipoles, an excitonic coupling between Chl-a2 and Chl-b2 was calculated^{61,62} to values between 120 and 180 cm^{-1} . At least the site Chl-a2 has been identified to be involved in fluorescence.⁶³ Therefore from fluorescence site selection measurements⁶⁴ of LHCII the relevant Huang–Rhys factor

times phonon-frequency for the Chl-a2 can be evaluated as $S\omega \approx 200 \text{ cm}^{-1}$. With this value one obtains an interaction parameter ν between 0.6 and 0.9. This means that the Chl-a2/b2 dimer, unlike the B820 subunit, could represent a subcritical case. However, for a Chl-a/b heterodimer the difference between the transition energy of Chl-a and Chl-b is around 400 cm^{-1} . Thus the site energy parameter Δ is nearly four times larger than in the case e (cf. Fig. 2), which represents an almost localized exciton. Hence, the Chl-a2/b2 heterodimer can be described in the same manner as a pair of uncoupled Chl-a and Chl-b molecules. Due to their experimental observation of a significant redistribution of oscillator strength to the fluorescent subband, Schubert *et al.*⁶² have suggested that the Chl-b2 site might be occupied by a Chl-a molecule instead of a Chl-b, i.e., the Chl-a2/b2 dimer is actually a homodimer (Chl-a2/a2'). In this case the excitonic coupling between the two sites is increased to around 220 cm^{-1} , resulting in $\nu \approx 1.1$. This is just above the critical value 1. Using a site energy parameter $\Delta \approx 0$, as they suppose, one obtains an effective delocalization of initially $L_{\text{eff}}(0) \approx 1.8$ and $L_{\text{eff}}(t \rightarrow \infty) \approx 1.5$. The first value has to be compared with the size enhancement of the absorption dipole, the latter with that of the emission.

It has to be noted that our estimates for both parameters, ν and Δ , are rather rough. This is particularly problematic in the vicinity of the critical case, where slightly different parameters will result in a completely different character of the exciton states.

ACKNOWLEDGMENTS

This work was supported by the Swedish Research Council and the Wenner–Gren Foundations.

- ¹J. I. Frenkel, *Phys. Rev.* **37**, 17 (1930).
- ²A. Davydov, *Theory of Molecular Excitons* (McGraw–Hill, New York, 1962).
- ³E. E. Jelley, *Nature (London)* **138**, 1009 (1936).
- ⁴E. W. Knapp, *Chem. Phys.* **85**, 73 (1984).
- ⁵H. Fidler, J. Knoester, and D. A. Wiersma, *J. Chem. Phys.* **95**, 7880 (1991).
- ⁶S. de Boer and D. A. Wiersma, *Chem. Phys. Lett.* **165**, 45 (1990).
- ⁷R. Monshouwer, M. Abrahamsson, F. van Mourik, and R. van Grondelle, *J. Phys. Chem. B* **101**, 7241 (1997).
- ⁸H. van Amerongen, L. Valkunas, and R. van Grondelle, *Photosynthetic Excitons* (World Scientific, New Jersey, 2000).
- ⁹S. G. Johnson and G. J. Small, *J. Phys. Chem.* **95**, 471 (1991).
- ¹⁰T. Pullerits, M. Chachisvilis, M. R. Jones, C. N. Hunter, and V. Sundström, *Chem. Phys. Lett.* **224**, 355 (1994).
- ¹¹V. Nagarajan, R. G. Alden, J. C. Williams, and W. W. Parson, *Proc. Natl. Acad. Sci. U.S.A.* **93**, 13774 (1996).
- ¹²M. Dahlbom *et al.*, *J. Phys. Chem. B* **104**, 3976 (2000).
- ¹³T. Pullerits, M. Chachisvilis, and V. Sundström, *J. Phys. Chem.* **100**, 10787 (1996).
- ¹⁴D. Leupold *et al.*, *Phys. Rev. Lett.* **77**, 4675 (1996).
- ¹⁵R. Jimenez, S. N. Dikshit, S. E. Bradforth, and G. R. Fleming, *J. Phys. Chem.* **100**, 6825 (1996).
- ¹⁶M. Dahlbom, T. Pullerits, S. Mukamel, and V. Sundström, *J. Phys. Chem. B* **105**, 5515 (2001).
- ¹⁷K. Sauer *et al.*, *Photochem. Photobiol.* **64**, 564 (1996).
- ¹⁸V. May and O. Kühn, *Charge and Energy Transfer Dynamics in Molecular Systems* (Wiley–VCH, Berlin, 2000).
- ¹⁹A. Suna, *Phys. Rev.* **135**, A111 (1964).
- ²⁰S. Fischer and S. Rice, *J. Chem. Phys.* **52**, 2089 (1970).
- ²¹S. Higai and H. Sumi, *J. Phys. Soc. Jpn.* **63**, 4489 (1994).
- ²²O. Kühn and V. Sundström, *J. Chem. Phys.* **107**, 4154 (1997).
- ²³T. Renger and V. May, *J. Phys. Chem. A* **102**, 4381 (1998).
- ²⁴J. A. Leegwater, J. R. Durrant, and D. R. Klug, *J. Phys. Chem. B* **101**, 7205 (1997).
- ²⁵O. Kühn, V. Sundström, and T. Pullerits, *Chem. Phys.* **275**, 15 (2002).
- ²⁶T. Förster, *Ann. Phys. (Leipzig)* **6**, 55 (1948).
- ²⁷T. Förster, *Z. Naturforsch. A* **4a**, 321 (1949).
- ²⁸K. Mukai, S. Abe, and H. Sumi, *J. Phys. Chem. B* **103**, 6096 (1999).
- ²⁹G. D. Scholes and G. R. Fleming, *J. Phys. Chem. B* **104**, 1854 (2000).
- ³⁰T. Meier, Y. Zhao, V. Chernyak, and S. Mukamel, *J. Chem. Phys.* **107**, 3876 (1997).
- ³¹A. Damjanovic, I. Kosztin, and K. Schulten, *Phys. Rev. E* **65**, 031919 (2002).
- ³²V. Sundström, T. Pullerits, and R. van Grondelle, *J. Phys. Chem. B* **103**, 2327 (1999).
- ³³M. Chachisvilis, O. Kühn, T. Pullerits, and V. Sundström, *J. Phys. Chem. B* **101**, 7275 (1997).
- ³⁴T. Pullerits, T. Polivka, M. Chachisvilis, J. L. Herek, and V. Sundström, in *Photosynthesis: Mechanisms and Effects*, edited by G. Garab (Kluwer Academic, New York, 1998), pp. 33–37.
- ³⁵T. Polivka, T. Pullerits, J. L. Herek, and V. Sundström, *J. Phys. Chem. B* **104**, 1088 (2000).
- ³⁶K. Timpmann, Z. Katilene, N. W. Woodbury, and A. Freiberg, *J. Phys. Chem. B* **105**, 12223 (2001).
- ³⁷M. Dahlbom, W. Beenken, V. Sundström, and T. Pullerits, in *Biophysical Chemistry 2001 Proceedings* (Royal Society of Chemistry, London, in press).
- ³⁸J. C. Tully, *J. Chem. Phys.* **93**, 1061 (1990).
- ³⁹D. M. Burland and A. H. Zewail, *Adv. Chem. Phys.* **60**, 369 (1979).
- ⁴⁰F. van Mourik *et al.*, *Biochim. Biophys. Acta* **1059**, 111 (1991).
- ⁴¹J. Deisenhofer, O. Epp, K. Miki, R. Huber, and H. Michel, *Nature (London)* **318**, 618 (1985).
- ⁴²R. A. Friesner and R. Silbey, *J. Chem. Phys.* **75**, 3925 (1981).
- ⁴³R. L. Fulton and M. Gouterman, *J. Chem. Phys.* **41**, 2280 (1964).
- ⁴⁴M. Hayashi *et al.*, *J. Chin. Chem. Soc. (Taipei)* **46**, 381 (1999).
- ⁴⁵T. S. Rahman, R. S. Knox, and V. M. Kenkre, *Chem. Phys.* **44**, 197 (1979).
- ⁴⁶A. Matro and J. A. Cina, *J. Phys. Chem.* **99**, 2568 (1995).
- ⁴⁷H. W. H. Lee and M. D. Fayer, *J. Chem. Phys.* **84**, 5463 (1986).
- ⁴⁸R. Kumble, S. Palese, R. W. Visschers, P. L. Dutton, and R. M. Hochstrasser, *Chem. Phys. Lett.* **261**, 396 (1996).
- ⁴⁹A. Witkowski and W. Moffitt, *J. Chem. Phys.* **33**, 872 (1960).
- ⁵⁰R. L. Fulton and M. Gouterman, *J. Chem. Phys.* **35**, 1059 (1961).
- ⁵¹Y. J. Yan and S. Mukamel, *J. Chem. Phys.* **89**, 5160 (1988).
- ⁵²S. Mukamel, *Nonlinear Optical Spectroscopy*, 1st ed. (Oxford University Press, New York, 1995).
- ⁵³G. D. Scholes, X. J. Jordanides, and G. R. Fleming, *J. Phys. Chem. B* **105**, 1640 (2001).
- ⁵⁴U. Weiss, *Quantum Dissipative Systems*, 2nd ed. (World Scientific, Singapore, 1999).
- ⁵⁵W. M. Fain and J. I. Chanin, *Quantenelektronik, Physik der Maser und Laser* (B. G. Teubner Verlagsgesellschaft, Leipzig, 1969).
- ⁵⁶O. V. Prezhdo and P. J. Rossky, *J. Chem. Phys.* **107**, 825 (1997).
- ⁵⁷R. W. Visschers *et al.*, *Biochemistry* **30**, 2951 (1991).
- ⁵⁸T. Pullerits, F. van Mourik, R. Monshouwer, R. W. Visschers, and R. van Grondelle, *J. Lumin.* **58**, 168 (1994).
- ⁵⁹T. Pullerits, R. Monshouwer, F. van Mourik, and R. van Grondelle, *Chem. Phys.* **194**, 395 (1995).
- ⁶⁰W. Kühlbrandt, D. N. Wang, and Y. Fujiyoshi, *Nature (London)* **367**, 614 (1994).
- ⁶¹H. van Amerongen and R. van Grondelle, *J. Phys. Chem. B* **105**, 604 (2001).
- ⁶²A. Schubert *et al.*, *Biophys. J.* **82**, 1030 (2002).
- ⁶³H. Rogl and W. Kühlbrandt, *Biochemistry* **38**, 16214 (1999).
- ⁶⁴E. J. G. Peterman, T. Pullerits, R. van Grondelle, and H. van Amerongen, *J. Phys. Chem. B* **101**, 4448 (1997).